Single-Switch Boost-Buck DC-DC Converter for Industrial Fuel Cell and Photovoltaics Applications

Mahmoud Dhimish[1], Nigel Schofield[2]

[1] Department of Electronic Engineering, University of York, York YO10 5DD, UK

[2] Department of Engineering and Technology, University of Huddersfield, Huddersfield HD1 3DH, UK

Abstract

The realization of dc-dc converters performs a vital function in exploiting renewable energy sources such as solar photovoltaic (PV) and fuel cell applications. This paper demonstrates a single-switch unidirectional buck-boost dc-dc converter for continuous power flow control, excluding the hybrid switched-capacitor. The proposed converter utilizes a limited number of passive components, only four diodes and three inductors required, in addition to six capacitors. The converter can operate at a wide input voltage range with continues input current. The converter has experimented under real-time conditions with 660 W PV system. The obtained efficiency ranges from 93% to 98%. Furthermore, the converter has interfaced with 550 W fuel cell operated under different fuel pressure. The realized efficiency ranges from 91% to 97%. The maximum measured inductance current ripple is limited to under 0.70 A in both scenarios, whereas 0.16 V is the maximum output voltage ripple.

Keywords: dc-dc converter; renewable energy; fuel cell, PV system; buck converter; boost converter.

1. Introduction

The dc output is generated by renewable energy sources such as solar photovoltaic (PV), fuel cell, and wind turbines. A suitable dc-dc converter is sought for the interconnection with these renewable sources to attain a maximum power conversion/regulation and energy management purposes. On the other side of the problem, these renewable sources cannot meet the demand and auxiliary energy storage such as battery banks. Hence, customary dc-dc converters are placed between the energy source and the load to meet the specific requirements.

There are two classes of a dc-dc converter, (i) unidirectional and (ii) bi-directional. The unidirectional converters can be customized to become a bi-directional if the diodes in the circuit are placed by controllable power switches. In applying fuel cells, it is mandated to use a unidirectional dc-dc converter to reject reversed current from the converter to pass into the fuel cell. This is also the situation in industrial PV systems applications.

A multiple-input configuration dc-dc converter with a power flow control was proposed by Karthikeyan & Gupta [1]. The converter is based on a multi-level h-bridge configuration that can utilize a power transfer efficiency of nearly 90%; this converter has no current sharing strategy. It cannot work as a buck converter. The solution to this problem has been suggested by Du *et al.* [2] by using a parallel dc-dc buck converter configuration. The converter is based on two power switch, two inductors and a single capacitor. Despite the simplicity of the structure, this convert can achieve a power efficiency higher than 91%.

According to Hossain & Rahim [3], a comparison of different modulation and control strategies for nonreasoning single-phase dual-active-bridge (NSDAB) dc-dc converters. They found that the steady-state and transient performance of NSDAB converters can achieve high efficiency (>90%) when optimized with additional inductance. The same strategy has been used by [4] in analysing the performance of multiple buck dc-dc converter with continues power load.

Other exciting results demonstrated by [5, 6] suggest using multi-level control mechanisms to attain higher voltage gain of buck dc-dc converters. The limitation of these studies is that both did not consider the rapid real-time fluctuation of the input current, which could be a possible concern in such applications, including PV systems. In addition, the indirect sliding mode control for dc-dc converters has been proposed by H. Komurcugil et al. [7]. This scheme allows a sliding surface function based on the input current error. However, it is an excellent accomplishment; conventional control modes using FPGAs or data acquisition board (i.e., using LabVIEW) could efficiently aid this functionality without additional power electronics in the circuit.

As later, we will present our proposed dc-dc converter's functionality with PV and fuel cell application; it would be relevant to explore the latest dc-dc converters in both areas. Siouane *et al.* [8] proposed a buck/buck-boost converter that comprises three power switches, two inductors, and two capacitors to ideally function with PV systems. The proposed converter also has a fault-tolerant algorithm to protect the interconnection with the battery bank. The results show that the power efficiency is above 92%; however, this study's main drawback is the control algorithm's implementation complexity. This complexity has been drawn to attention by [9]-[11]; they proposed a simplistic yet efficient control model for PV converters. These algorithms are more suitable for multi-level buck dc-dc converters and more complex dc-dc converter such as LLC bidirectional dc-dc converter [12] or the non-isolated buck-boost dc-dc converter as proposed by Gorji *et al.* [13].

A limited number of dc-dc converters function under a single power switch; in practice, this would decrease the converter's design complexity and can be operated with least control. Azer & Emadi [14] proposed a multi-phase buck-boost converter using a single power switch. The converter (for every phase) requires a single inductor and resistor. Output capacitance is the need for the current drive when the power switch is turned off. Another interesting buck/buck-boost that has a single-switch was proposed by Litrán *et al.* [15]. The converter requires two inductors, four diodes and three capacitors. In Both studies, [14, 15], the converter efficiency ranges between 85% ~ 90% under varying load conditions.

Many recent studies utilize dc-dc converters with fuel cells. Huangfu *et al.* [16] proposed a buck-boost converter comprising four power switches, two inductors and two capacitors. The converter was experimented with under different input voltage and output current, while measured efficiency ranging from 92% up to 95.8%. In contrast, a comparable converter was formed by Diaz-Saldierna *et al.* [17] but with more passive components. The peak measured efficiency of this converter is limited to 92%.

The limitation with studies related to dc-dc converter integration with fuel cells [16]-[21] assumes that the fuel cell has a single voltage-current profile. Whereas in practice, as the fuel pressure varies, the voltage-current characteristics differ. For example, when utilising low pressure (0.1 bar or below), the output voltage at full load drops significantly. This challenge must be a standing proposal for us to consider in our work.

In this article, we will present the development of a single-switch unidirectional buck-boost dc-dc converter. The proposed converter can operate under continuous input current, making the converter capable of integrating with renewable sources. The converter's examination with a 660 W PV system under real-time long-term condition was performed in such a case. We have also integrated the converter with a 550 W fuel cell while varying the fuel pressure (0.5 to 0.1 bar). The steady-state analysis of the converter is explained along with the multiple operational modes.

2. Working Principle of the Proposed Converter

The circuit diagram of the proposed dc-dc converter is shown in Fig. 1. The developed converter is a single-switch non-isolated, making it advantageous and easy to control because only two states in the working condition are available when the switch is turned ON or OFF. The converter comprises a power switch, three diodes, four inductors and six capacitors.

The converter's main power switch is employed as an ideal so that the parasitic capacitance can be neglected; current state-of-the-art power switches can aid this assumption. The converter has two main operational modes, continues conduction mode (mode #1) and the discontinues conditions mode (mode #2). Both operational modes of the converter are explained as follows:

2.1 Continues conduction mode (mode #1)

During mode #1, the converter's power switch is turned ON; consequently, diodes $D1$, $D3$, and $C4$ in the circuit are OFF. The linear magnetization of the inductors is now operational. The first capacitor, $C1$, is in discharging mode. While capacitor, $C2$, is now being charged by $C3$; similarly, $C4$ is being charged by $C5$. The flow of the current is displayed in Fig. 2(a). The voltage across the inductors can be formulated as (1)-(2).

$$V_{L1} = V_{input} \tag{1}$$

$$V_{L2} = -V_{C1} = -V_{input} \tag{2}$$

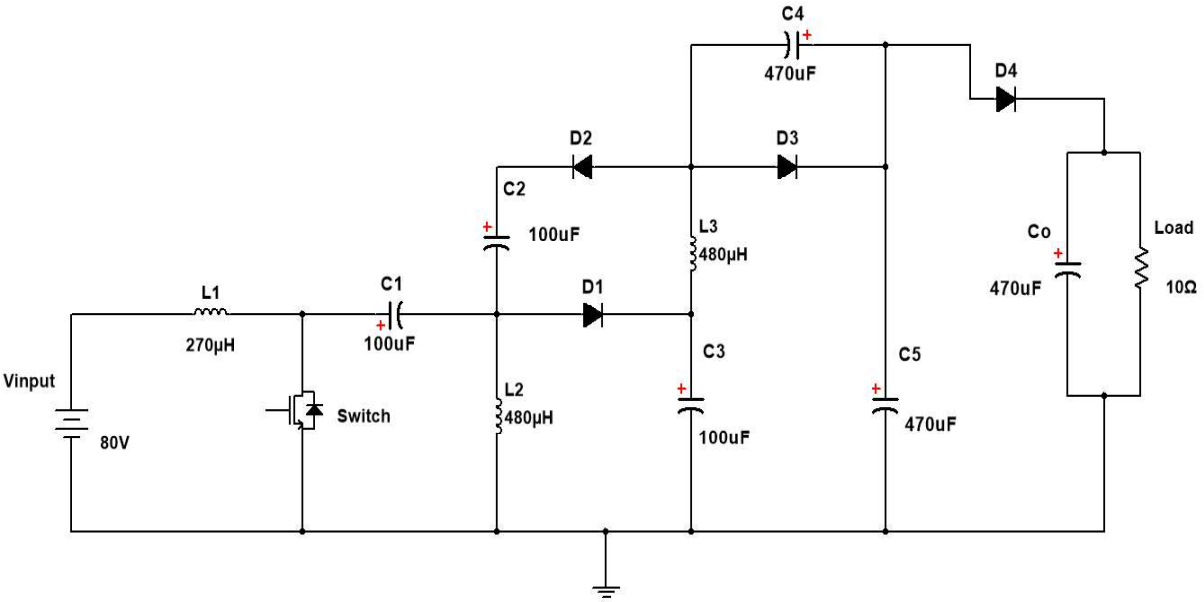

Fig. 1 - Equivalent circuit of the proposed converter.

The current flowing into each capacitor can also be formulated using (3)-(6). The maximum current would be exacted across capacitor $C1$, whereas a negative current appears in capacitor $C4$.

$$i_{C1} = -i_{L2} - i_{C2} - i_{C3} = -3\, i_{load} \tag{3}$$

$$i_{C2} = -i_{C3} = i_{L3} = i_{load} \tag{4}$$

$$i_{C4} = -i_{C5} = i_{load} \tag{5}$$

$$i_{Co} = -i_{load} \tag{6}$$

It is worth noting that the diode ($D2$) allows having a track to discharge $C3$ into $C2$ while using a common ground in the circuit.

2.2 Continues conduction mode (mode #2)

During mode #2, the converter's power switch is turned OFF; consequently, the four diodes in the circuit are ON. The linear demagnetization of the inductors is now operational. The inductor $L1$ now charges the capacitor $C1$. The inductors $L2$ and $L3$ are charing both $C3$ and $C5$, respectively.

The reaming capacitors, $C2$ and $C4$, are directly being discharged. The flow of the current is displayed in Fig. 2(b). The voltage across the inductors can be formulated as (7) and (8) with respect to the duty cycle, D.

$$V_{L1} = \frac{-D}{1-D} V_{input} \tag{7}$$

$$V_{L2} = V_{L3} = \frac{+D}{1-D} V_{input} \tag{8}$$

The current flowing into each capacitor can be expressed using (9)-(11). The maximum current is expected to be across the capacitor C1.

$$i_{C1} = \frac{3D}{1-D} i_{load} \tag{9}$$

$$i_{C2} = i_{C3} = \frac{-1}{1-D} i_{load} \tag{10}$$

$$i_{C4} = i_{C5} = \frac{-D}{1-D} i_{load} \tag{11}$$

For both Mode #1 and Mode #2, it is worth to mention that the value of the capacitors is large; hence, the constant voltage across the capacitors can be considered. Form the consideration of the circuit design; we can notice that the developed converter has the following key features, (i) it is derived from conventional SEPIC converter as one power switch is used, (ii) limited combinational number of capacitors and inductors are used, and (iii) the proposed converter has the ability to function under continues input current.

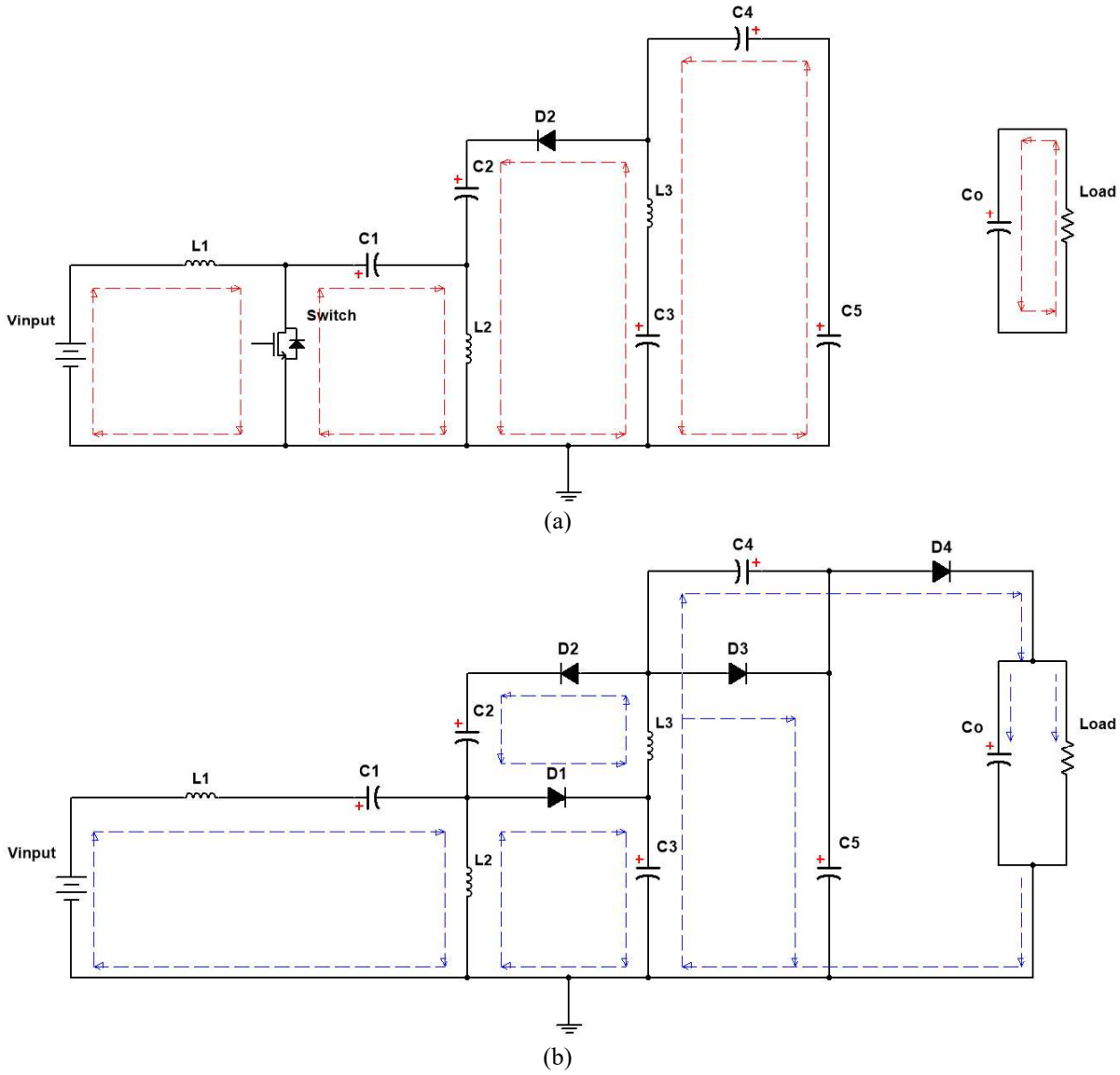

Fig. 2 - Working modes of the proposed converter. (a) When the power switch is ON, Mode #1, (b) When the power switch if OFF, Mode #2.

The typical output voltage (vs. time) of the inductors are shown in Fig. 3(a), the drop in the voltage at $(1-D)T_s$ is equal to $\frac{-D}{1-D}V_{input}$; in addition, the maximum observed voltage of the power switch is equivalent to $\frac{V_{input}}{1-D}$, this is relatively small voltage drop maximizing the converter while operating at buck conversion mode having minimal losses in the voltage.

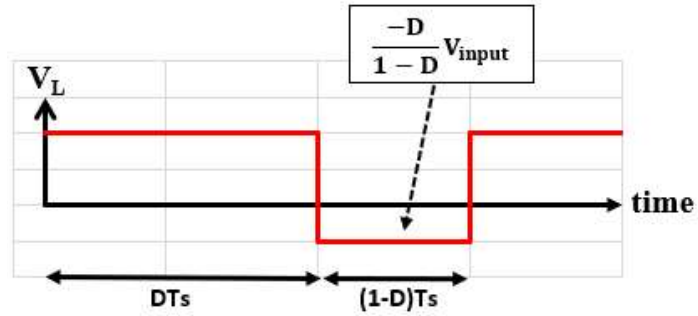

(a)

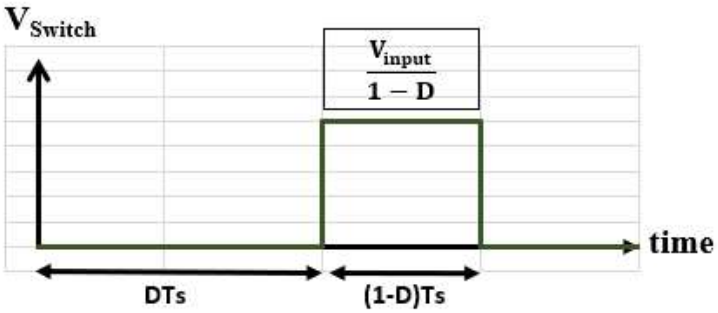

(b)

Fig. 3 - Typical waveforms of the signal. (a) Indicator's voltage, (b) Power switch voltage.

3. Voltage Gain Analysis

To find the voltage the converter's voltage gain with respect to the duty cycle, we must apply the voltage-second balance principle to inductors. This is where we integrate the actual voltage changes throughout the sampling frequency ($\frac{1}{T_s}$). The voltages of the inductor have been summarized earlier in (1)-(2) and (7)-(8). Therefore, we can find the relationship between the input and the output voltage, as presented in (12).

$$V_{input} = \frac{1-D}{D} V_{C5} \tag{12}$$

We know that the voltage across $C5$ capacitor is equal to twice the voltage across $C4$. Hence, we can simplify this in (13) to obtain the voltage in the output (load).

$$V_{load} = V_{output} = 2V_{C5} = \frac{3D}{1-D} \tag{13}$$

The output voltage gain of the proposed converter is shown below:

$$Voltage\ Gain = \frac{V_{output}}{V_{input}} = \frac{3D}{1-D} \tag{14}$$

The voltage gain against the duty cycle of the proposed dc-dc converter is presented in Fig. 4. We can observe that the converter achieves higher voltage gain than conventional buck dc-dc converter and recent refined buck dc-dc converters proposed by [2] and [8].

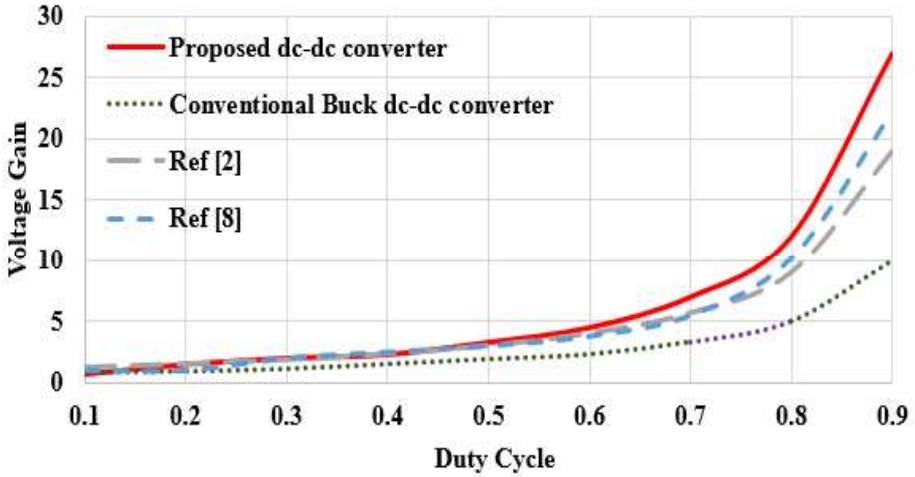

Fig. 4 - Voltage gain vs duty cycle of the proposed dc-dc converter compared with other recent converters.

4. Discontinues and the Boundary Conduction Modes

The inductors current in the energy transfer never reach zero value during the continuous condition modes (mode #1 and mode #2) shown earlier in Fig. 2. However, in the discontinues condition mode (DCM), the inductors' current falls to zero level, which is very popular in the single-switch converter.

The proposed converter's discontinuous condition mode occurs when the diodes ($D1$, $D2$ and $D3$) and all the inductors' current is equal to zero; therefore, no voltage is across the inductors, whereas the current flow is marked on Fig. 5(a). The total inductance in the circuit is as follows:

$$L_{Total} = \frac{1}{L_1} + \frac{1}{L_2} + \frac{1}{L_3} \tag{15}$$

During the discontinuous condition mode, the converter's voltage gain is equal to (16). It is observed that the voltage gain depends not only on the duty cycle (D) but also on the total inductance (L_{Total}), load resistance (R) and the T_s.

$$Voltage\ gain = \frac{V_{output}}{V_{input}} = \frac{D}{\tau 1} = \frac{D}{\sqrt{\frac{2\,L_{Total}}{R\,T_S}}} \tag{16}$$

When the normalized inductor time constant ($\tau 2$) is obtained (see equation 18 and Fig. 5(b)), the converter will operate under the boundary conduction mode. At this mode, the circuit detects whether the converter is running under the discontinuous or the continues condition mode, hence, adjusting the power switch and the duty cycle.

$$\tau 2 = \frac{(1-D)^2}{9} \tag{17}$$

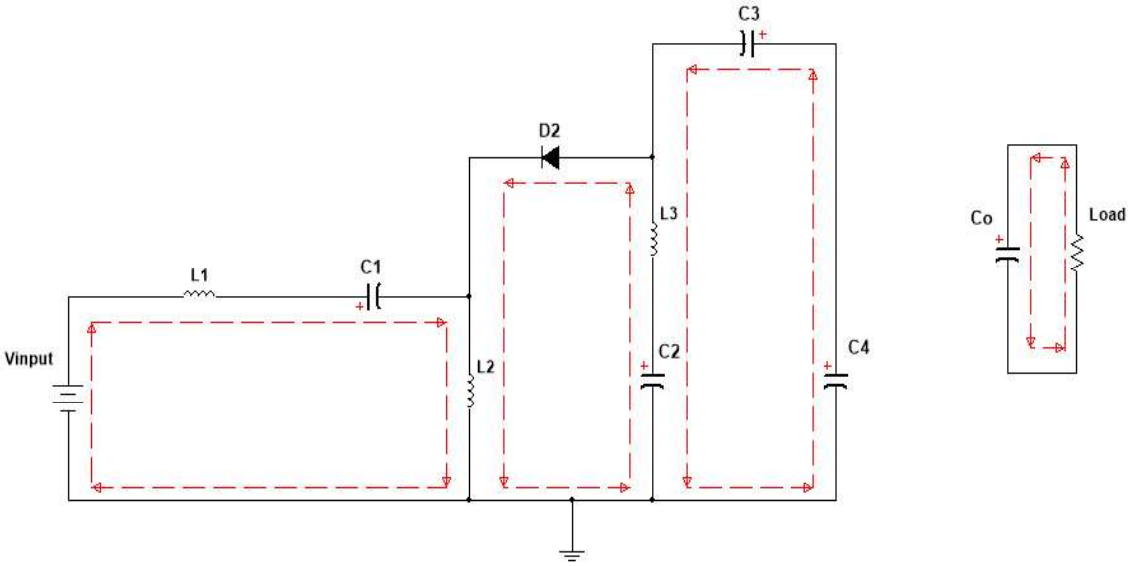

(a)

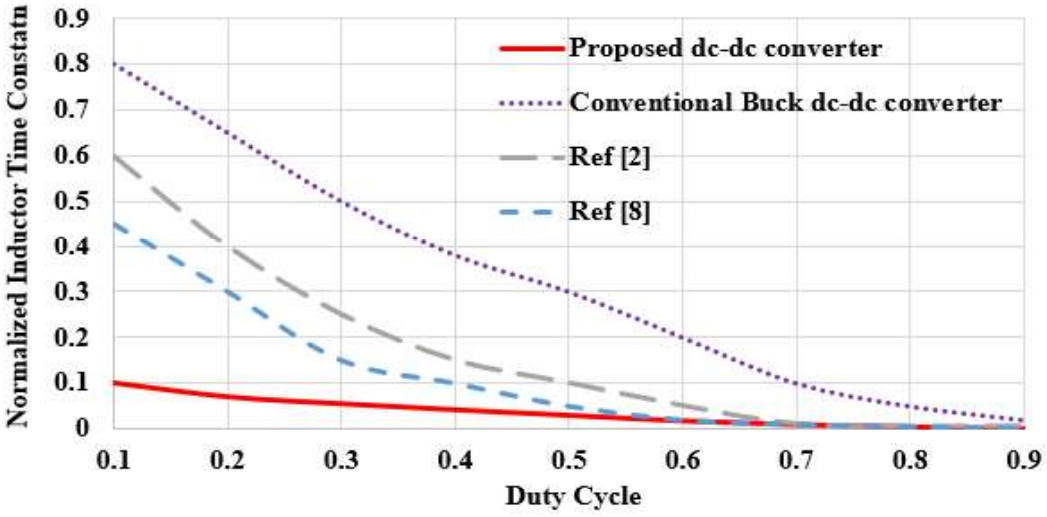

(b)

Fig. 5 - (a) Current flow of the converter during the discontinuous conduction mode, (b) Normalized inductor time constant vs duty cycle.

5. Converter Power Loss Estimation

It is crucial not only to analyse the conduction modes of the dc-dc converter but also to evaluate the circuit's total power loss. Four primary losses are observed, including the power switch loss, losses in the capacitors, conduction losses of inductors, and the diodes' losses.

The power switch loss is equal to (18). It comprises the switching frequency, input voltage, duty cycle, output current and the $R_{DS(on)}$ of the selected switch available in the manufacturer datasheet.

$$Switch_{loss} = \frac{f_S C_s (V_{input})^2 + R_{DS(on)} 9D (i_{output})^2}{(1-D)^2} \quad (18)$$

The losses in the capacitors are formed using (19), while the inductors' conduction losses are equal to (20).

$$Capacitance_{loss} = loss\ in\ C1 + Loss\ in\ the\ remaining\ capacitors = \frac{9D}{1-D}(i_{output})^2 + 5\ \frac{D}{1-D}(i_{output})^2 \quad (19)$$

$$Inductance_{loss} = Loss\ in\ L1 + loss\ in\ the\ remaining\ inductors = \frac{3D}{1-D}(i_{output})^2 + 2\ (i_{output})^2 \quad (20)$$

The diodes have two losses, the forward resistance and forward voltage (here, we considered 0.7 V as the silicon diodes have been used). Both can be determined using the combine equation (21).

$$Diode_{loss} = Forward\ resistance + forward\ voltage = Resistive\ load\ \frac{(i_{output})^2}{1-D} + 0.7\ i_{output} \quad (21)$$

In summary, the dc-dc converter's total power losses are the sum of the losses calculated using (18)-(21). We will assess the dc-dc converter's performance in the next sections, considering the total losses, output power, and efficiency.

6. Converter Duty Cycle Control

The duty cycle of the converter is controlled using the LabVIEW data acquisition board (DAQ 6001). To attain the required duty cycle for the converter, the following pseudo-code has been created,

pseudo code of the duty cycle control for the proposed converter

---

Start

Set $Voutput = 36$;

While ()

{

measured $Vinput$

$D = \frac{Voutput}{Vinput}\left[\frac{1}{3+\frac{Voutput}{Vinput}}\right]$

{

If $D > 0$

Set D // here the duty will be generated to the power switch

Else

$D = 0$ // here the output voltage is zero

}

}

// $D\ (minimum) = \frac{36}{105}\left[\frac{1}{3+\frac{36}{105}}\right] = 0.10$

// $D\ (maximum) = \frac{36}{21}\left[\frac{1}{3+\frac{36}{21}}\right] = 0.36$

Depends on the input voltage level, the duty cycle will be adjusted. For example, as discussed in the next section, the PV system operates from 21 V to 86 V. Hence, the duty cycle ranges from 0.12 and 0.36. Similarly, for the fuel cell system, the voltage range is 52 to 105; therefore, it will be required to control the duty cycle between 0.1 to 0.19.

The modelling of the proposed converter was made using NI Multisim simulation software. Appendix A shows the converter working at buck mode (80 V to 36 V), Appendix B presents the converter while running at boost mode (21 V to 36 V).

7. Results and Discussion

7.1 Converter Testing with 660 W PV system

The converter is connected with a string of PV modules comprising three series-connected polycrystalline silicon PV modules, as shown in Fig. 6. The PV system main electrical parameters are as follows:

1) PV string maximum output power: 660 W
2) Maximum output voltage: 86 V
3) Maximum output current: 7.67 A

The converter output pins are connected with a load (a combinational of a three-series battery bank (36 V) and pure resistive load). The converter's voltage/current input/output is monitored using LabVIEW software using DAQ6001, while the converter's component ratings are available in Table 1.

Table 1 - Proposed converter's component ratings

Parameter	Value (unit)
Rated Power	660 W
Maximum Input Voltage	120 V
Output Voltage	36 V (buck operation)
Power Switch	IRFP4668PBF
Inductor $L1$	270 µH
Inductors $L2$ and $L3$	480 µH
Capacitors, $C1, C2, C3, C4$	100 µF
Capacitors, $C5, Co$	470 µF
Diodes, $D1, D2, D3$ and $D4$	RURG5060 (600V, 50A)
Power Switch Driver	DAQ6001 LabVIEW
Switching Frequency	75 kHz

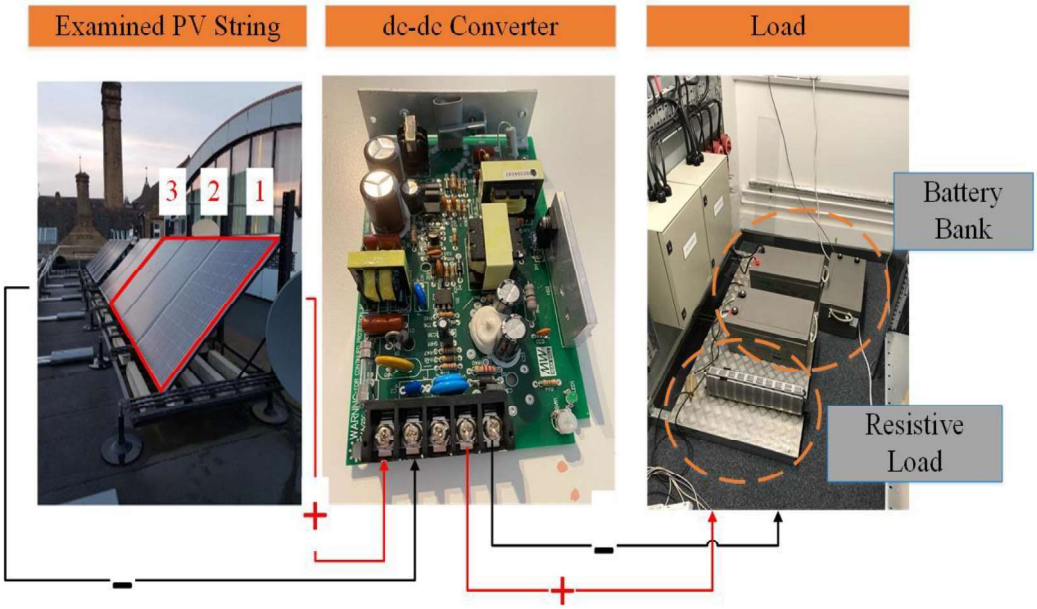

Fig. 6 - PV system connected with the proposed converter.

It is worth discussing that we have contemplated this interconnection rather than using "dummy" laboratory setup. The results would be further relevant to comprehend, and the converters' efficiency would be contained under real-time PV operating conditions, rather than using an indoor programmable load [10]-[12].

The output measured power, current and voltage of the PV string are shown in Fig. 7. As we can recognise, the PV string started to generate power at 6:07 before going to off-mode again after 18:47. The maximum capacity of 575 W has been delivered at the peak time, 12:16. The current and the output power increases as the irradiance increase, while the PV string output voltage varies from 57.3 V to 85.4 V.

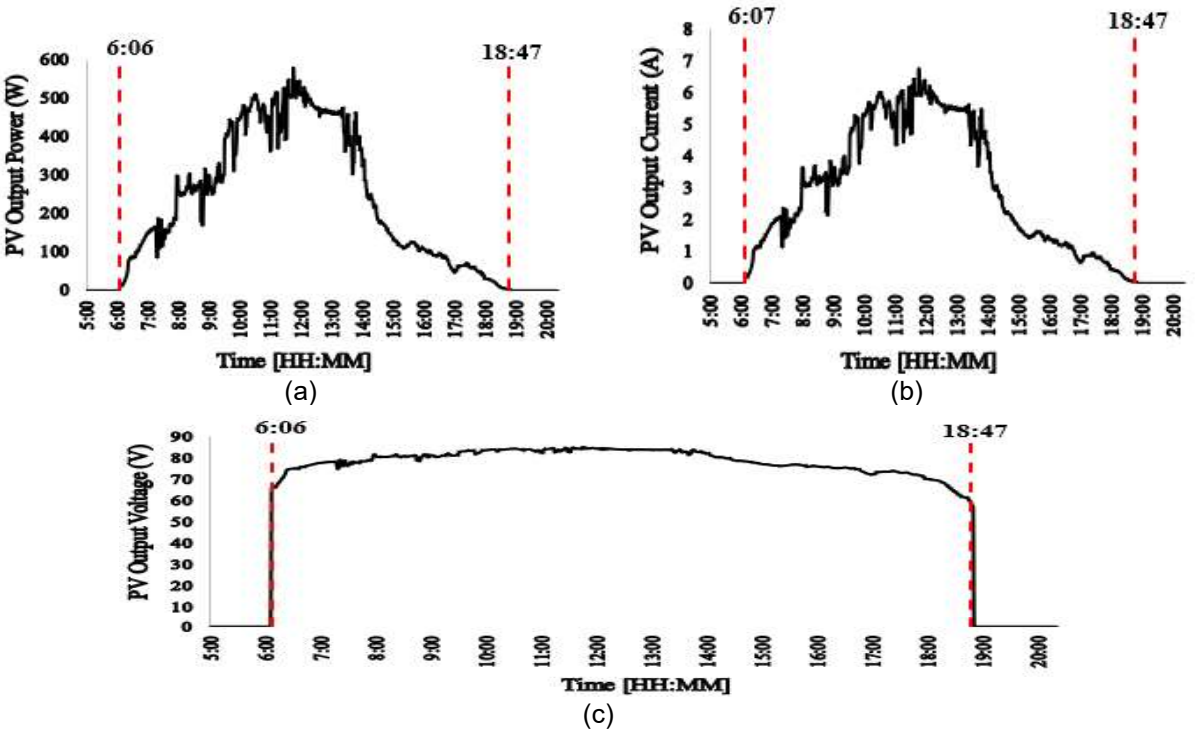

Fig. 7 - PV output “converter input”. (a) Power, (b) Current, (c) Voltage.

During this experiment, the resistive load is equal to 10 Ω. The converter's output voltage is shown in Fig. 8(a), achieving the desired output of 36 V (equivalent to the battery bank required voltage); at an ideal condition, the output voltage is obtained using (22). The transient response (in 50 μs) reads the output voltage ripple of 0.16 V.

$$V_{output} = \frac{3 \times D}{1-D} \times V_{input} = \frac{3 \times 0.125}{1-0.125} \times 84 = 36\,V \qquad (22)$$

Now let observe the inductors current ripple (see Fig. 8(b)). Continues current is performed, which confirms our introductory exploration of the converter in the previous sections.

The output current ripple of the input inductor $L1$ and the output inductors $L2$ and $L3$ can be obtained using (23) and (24), respectively. Nearly agree with the experimental results in Fig. 8(b). The average current value of $L1$ is equal to 5.65 A, while $L2$ and $L3$ have an average current of 6.9 A. For the calculation, the relevant parameters' values are reacquired from Table 1.

$$\Delta i_{L1} = \frac{D \times V_{input}}{L1 \times f_S} = \frac{0.125 \times 84}{270 \times 10^{-6} \times 75 \times 10^{+3}} = 0.52\ A \quad (23)$$

$$\Delta i_{L2\ and\ L3} = \frac{D \times V_{input}}{L2,L3,L4 \times f_S} = \frac{0.125 \times 84}{480 \times 10^{-6} \times 75 \times 10^{+3}} = 0.29\ A \quad (24)$$

The converter efficiency at varying input voltages is presented in Fig. 8(c). Here, we show that the average efficiency at the varying load current is equal to 96.5% when the input voltage is equal to 75 V. Besides, when the input voltage is at worst case condition, 85 V, the average efficiency is slightly dropped to 94.7%

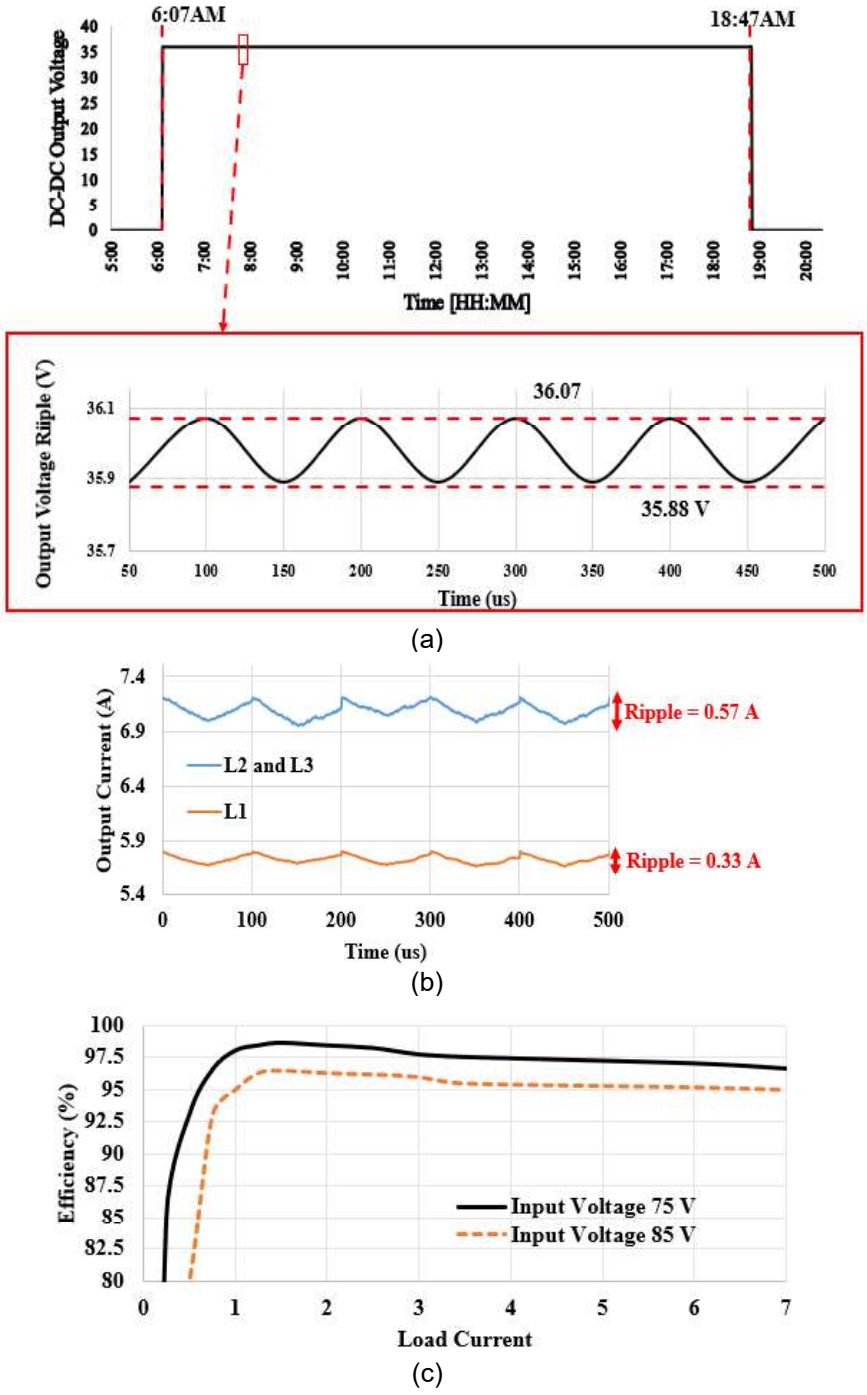

Fig. 8 - (a) The converter's output voltage, (b) Inductor L1, L2 and L3 current transient response, (c) The converter's output efficiency at varying input voltage level.

7.2 Converter Testing with 550 W Fuel Cell

A 500 W hydrogen PEM fuel cell (Fig. 9(a)) is utilised to extend the proposed converter's evaluation. The fuel cell requires near pure (0.99) hydrogen gas at a standard gauge pressure of 0.5 bar (maximum 0.75 bar). The low-pressure hydrogen supply is taken from compressed, 175 bar hydrogen gas, as shown in Fig. 9(b). The controls, overpressure safety vents, purge and drain points are all installed.

The fuel cell test chamber and the resistive load bank is shown in Fig. 9(c). The fuel cell's voltage-current characteristics are presented in Fig. 9(d). The fuel cell's output voltage ranges from 52 Vdc to 105 Vdc, depending on the fuel pressure (maximum is 0.5 bar), while the maximum output current is 8 A. Key characteristics of the fuel cell are presented in Table 2.

The fuel cell was connected to a purely resistive load via the proposed converter to regulate the input voltage to an output voltage of 36 V. The fuel cell has a continues working cycle; this is not a concern as the converter servers this functionality.

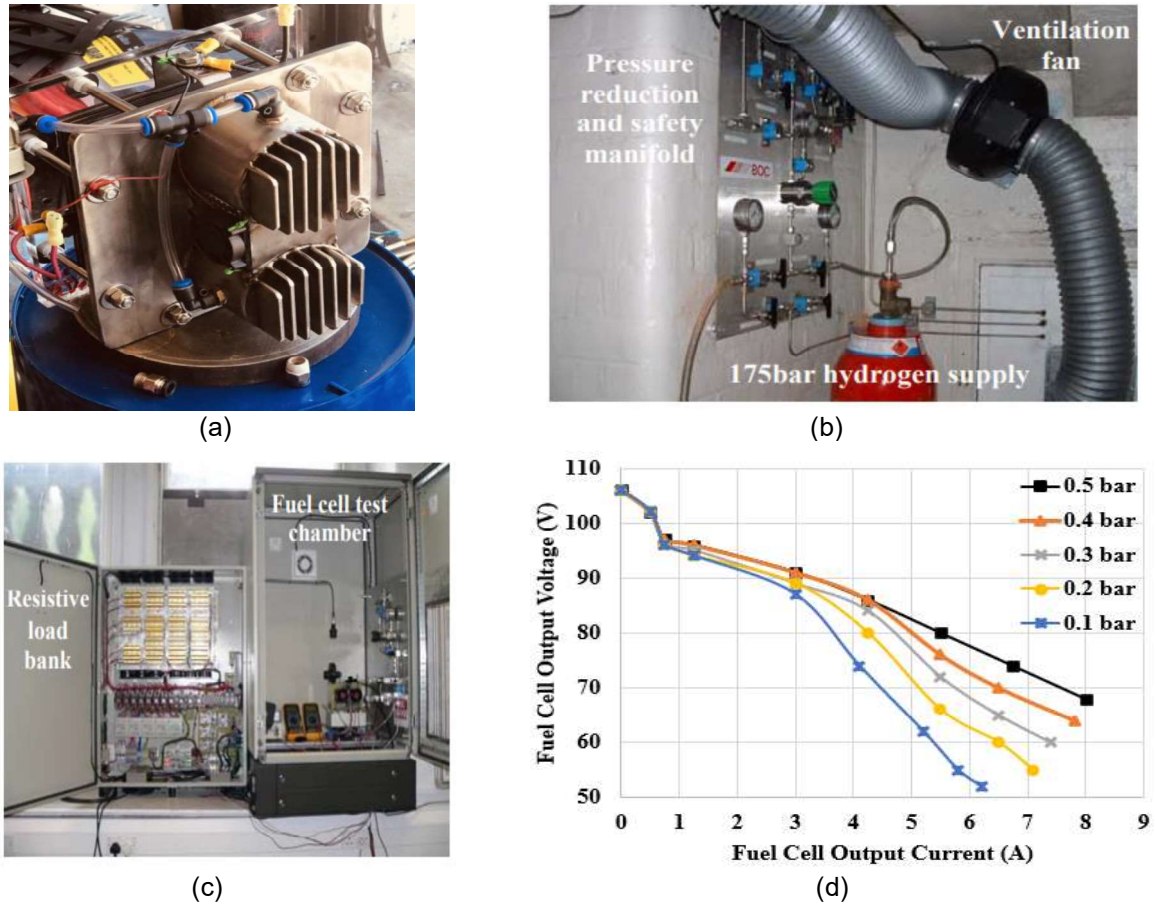

(a) (b) (c) (d)

Fig. 9 - (a) Fuel cell setup, (b) Fuel cell hydrogen supply, (c) Resistive load and the fuel cell chamber, (d) Fuel cell V-I characteristics under varied fuel pressure.

Table 2 - Fuel cell key characteristics

Parameter	Value (unit)
Unregulated output voltage range	52 – 105 Vdc
H_2 consumption at full-load	39 L/min (0.2 Kg/h)
Maximum rated output power	550 W
Total Number of cells	120 (2 x 60 per stack)
Maximum Stack temperature	69 ˚C
Fuel supply	Pure hydrogen (0.99)
Working cycle	Continuous

The converter has experimented under a varying fuel pressure (0.5 bar to 0.1 bar, see Fig. 9(d)). This experiment is unique as we have marked multiple recent studies [16]-[19] imply a steady fuel cell voltage, where in reality, it is unstable depending on the applied fuel pressure. Besides, the resistive load was also varied to investigate the loading settings. This experiment's prime objectives are (i) to verify whether the proposed converter can regulate the output voltage to 36 V with the smallest output voltage ripple and (ii) to investigate the efficiency of the converter under varying fuel pressure.

The output power vs output current of the fuel cell is given in Fig. 10(a). The maximum output power is 550 W; this result verifies that the proposed converter can be connected with the fuel cell as its full peak power is 660 W.

While varying the fuel pressure (0.5 bar to 0.1 bar), the output fuel cell voltage was measured and displayed in Fig. 10(b). Each fuel pressure variation operated for 20 seconds (as advised by the manufacturer datasheet). Remarkably, the converter's average output voltage is equal to 35.98 V with a maximum voltage ripple of 0.12 V.

The output current ripple of the inductor $L1$ and the inductors $L2$ and $L3$ can be obtained at 90 V fuel cell voltage using (25) and (26), respectively. The inductors current ripple is below 0.75 A, which is similar to our previous findings with the PV system (see (23) and (24)).

$$\Delta i_{L1} = \frac{D \times V_{input}}{L1 \times f_S} = \frac{0.125 \times 90}{270\times10^{-6}\times75\times10^{+3}} = 0.56\ A \quad (25)$$

$$\Delta i_{L2\ and\ L3} = \frac{D \times V_{input}}{L2,L3,L4 \times f_S} = \frac{0.125 \times 90}{480\times10^{-6}\times75\times10^{+3}} = 0.31\ A \quad (26)$$

The converter efficiency at different fuel cell pressure is shown in Fig. 10(c). We observed that the average efficiency at the varying load current is altering from 96.6% to 93.8%. The lowest efficiency (91.2%) was witnessed when the fuel cell pressure is most downward (0.1 bar) at full load.

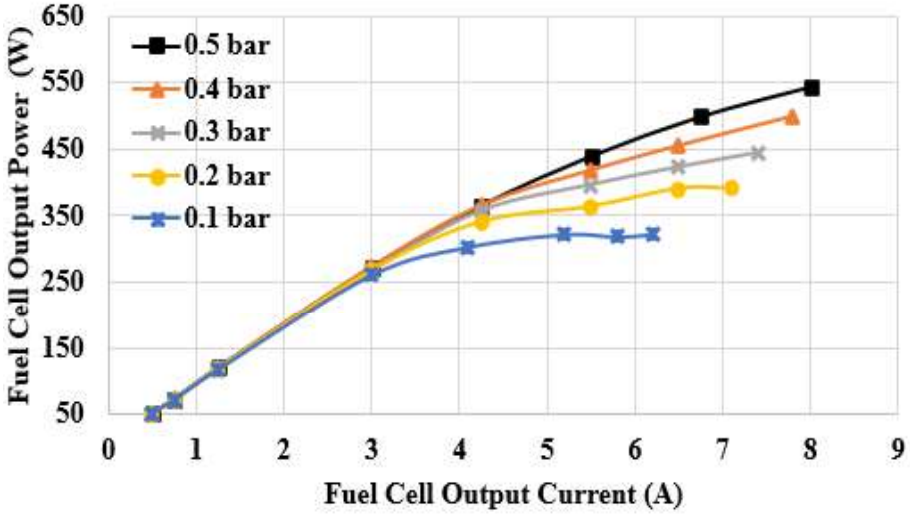

(a)

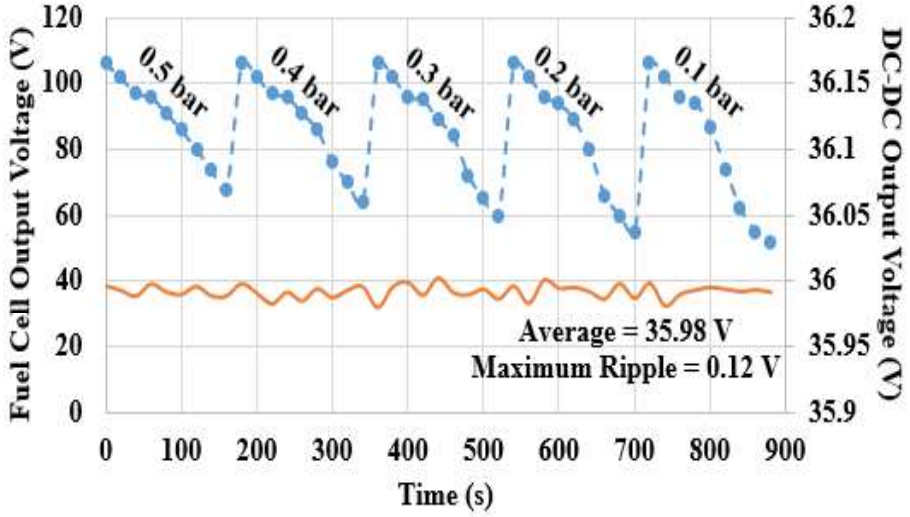

(b)

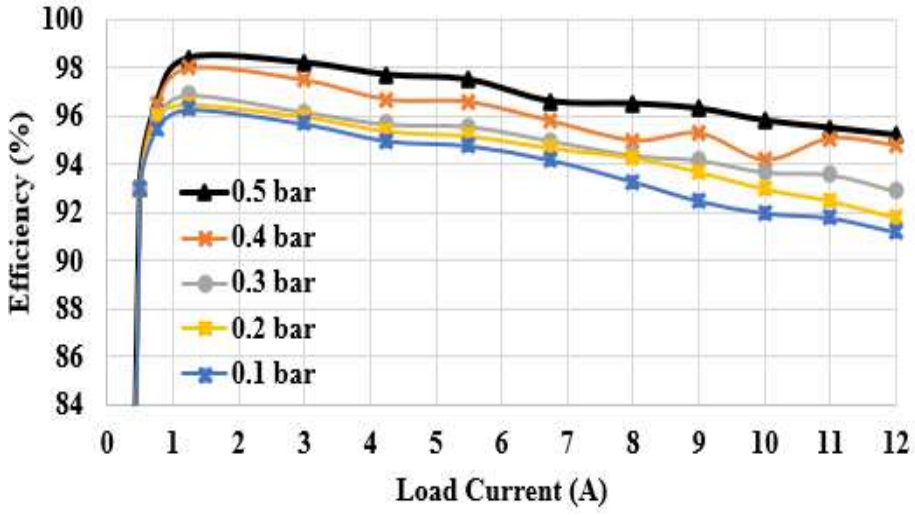

(c)

Fig. 10 - (a) Fuel cell output power vs output current, (b) Fuel cell output voltage vs the converter output voltage, (c) Converter efficiency vs load current (five curves represents the fuel cell operating at variable fuel pressure).

7.3 Summary of the Results

The efficiency of the converter while operating at different conditions are summarized in Fig. 11. When the converter is connected with the PV system, we observed that the efficiency is always greater than 94% at varying solar irradiance and output voltage (Fig. 11(a)). The only case where the efficiency dropped to almost 93% is when the output rated voltage is 85V, and the irradiance is at a peak, 1000 W/m^2. Here the PV system temperature was 23˚C. Please note that in Fig. 11, the output voltage corresponds to the voltage of the PV system or fuel cell, not the output voltage of the converter, which is regulated at 36 V.

In contrast, the converter efficiency is imperceptibly dropped when connecting with the fuel system (Fig. 11(b), yet in most cases, it is greater than 94%. In addition, at minimal fuel pressure (0.1) and maximum operating voltage (85V), a maximum drop in the converter efficiency was detected at 91%.

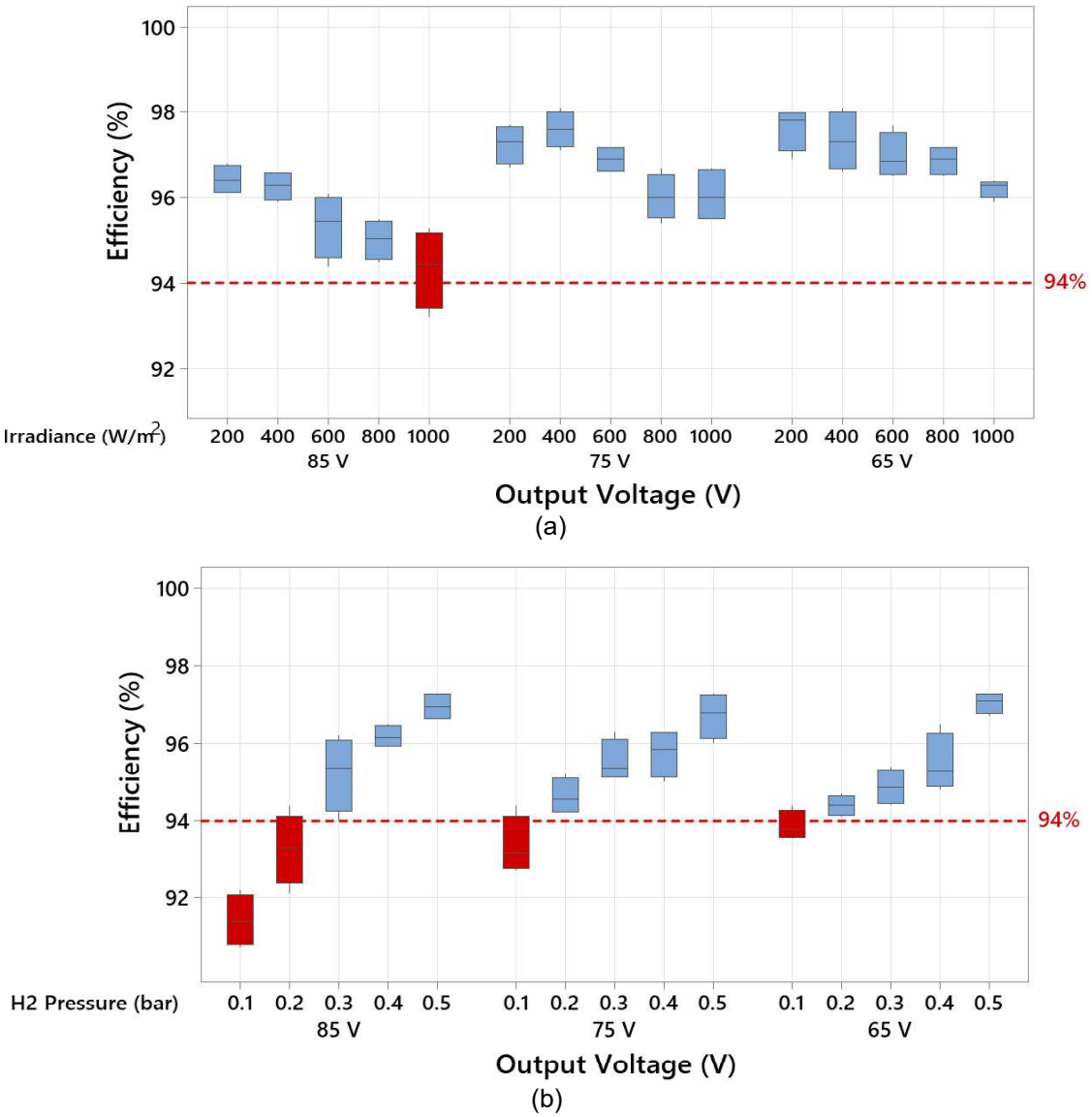

Fig. 11 - Proposed Converter efficiency at (a) varying solar irradiance and output voltage of PV system, (b) Varying the H_2 pressure and output voltage of the fuel cell.

Besides presenting the overall power losses obtained from the converter efficiency, a study about the power loss was also made. This critical analysis points out the components that dominate the power-losses in the proposed convert design. Fig. 12 shows the power-loss breakdown at full load conditions, considering the power semiconductors conduction calculated using (20), switching losses computed using (18), and magnetic devices losses calculated using (19) and (21), including other losses, i.e., temperature-dependent losses in the components wire losses, and proximity and skin effect losses. We have not considered the gate drive power loss as it can be included within the other losses estimation [23 ,24].

When the converter is connected to the PV system (Fig. 12(a)), the total power loss is equal to 9.2 W compared with 10.5 W when connected with the fuel cell (Fig. 12(b)). This is because the conduction losses are higher than the switching losses. In contrast, if we consider Fig. 12(b), as the fuel cell requires a reverse switching mechanism, the losses were nearly identical for the condition and the switching. In contrast, The maximum voltage stress of the power switch is expressed by (27), which is closely approves with the experimental results in Fig. 12 (c).

$$V_{stress,swtich} = \frac{V_{output}}{1-D(maximum)} = \frac{36}{1-0.36} = 56.25\ V \tag{27}$$

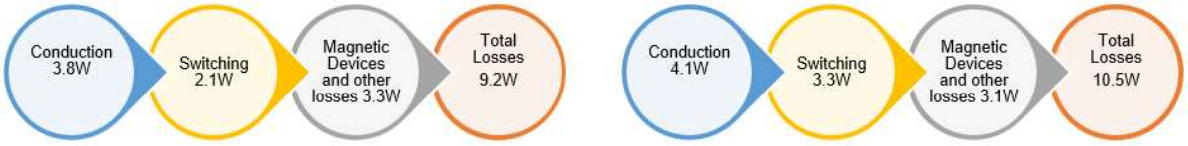

(a) (b)

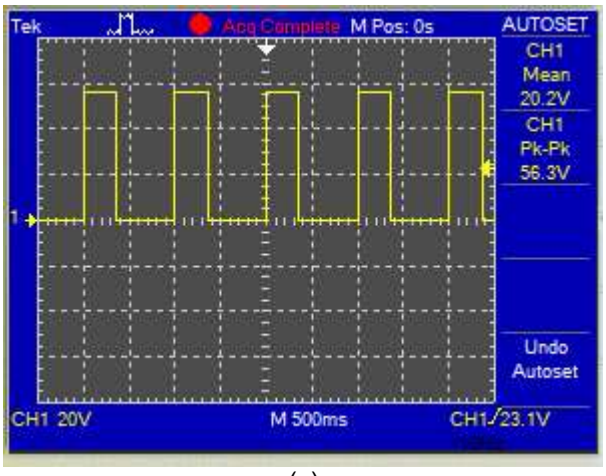

(c)

Fig. 12 – (a) Power loss at full load PV condition, (b) Power loss at full load fuel cell condition, (c) Maximum observed voltage stress across the power switch.

For thermal performance evaluation, we have taken the thermal images of the converter under full load conditions while connected with the PV system (Fig. 13(a)) and the fuel cell (Fig. 13(b)). These images were taken using a FLIRi7 thermal camera with thermal sensitivity ±0.1˚C. We observe no overheating in the converter component in both cases, while the temperature is approximately 50˚C.

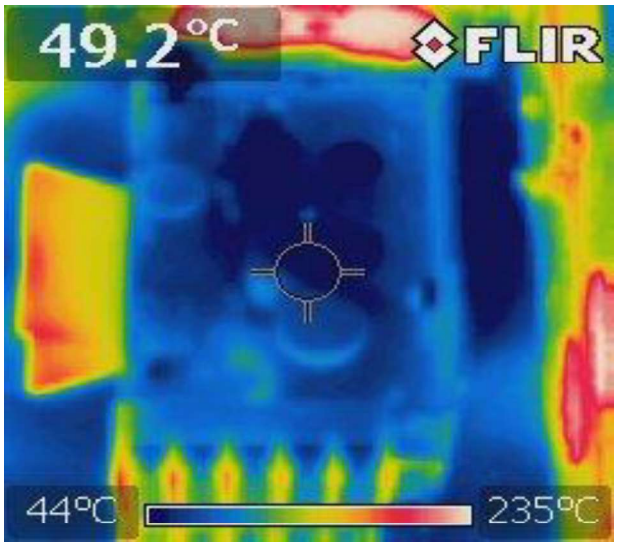

(a)

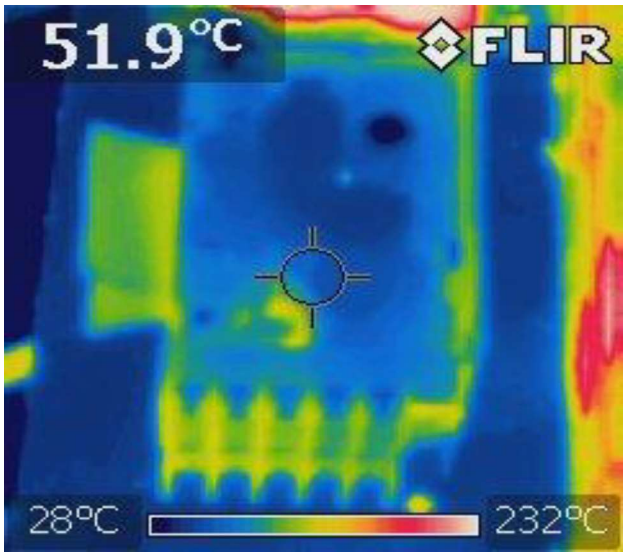

(b)

Fig. 13 - Thermal images of the converter operating at full load conditions connected with (a) PV system, (b) fuel cell.

Last but not least, a comparison of the proposed converter with converters introduced in [15] and [25, 26] is presented in Table 3. According to the comparative study, our converter's voltage gain is suitable and has fewer complications than [15] or [25]. Hence, we have successfully implemented the converter using a singular power switch, requiring limited control of the ON/OFF state for the switch. Compared with [26], our proposed converter has greater efficiency, particularly while integrating with fuel cells at varying pressure. Despite that, [26] has a good performance. However, they have not compared their converter efficiency while varying the fuel pressure. In addition, even though the number of elements in the proposed converter is higher than all previously proposed converters, we have achieved greater power efficiency with sufficient voltage gain with minimum power losses.

Furthermore, we have not noticed a previously published work on a dc-dc converter, including a single-switch mechanism experimentally validated using PV and fuel cell application. This adds to the advantage of our proposed converter and the overall design and experimental verification demonstrated in our study.

Table 3 - Comparative results of the proposed dc-dc converter with recently published work [15] and [25, 26].

Parameter	Proposed Converter	Ref. [26]	Ref. [25]	Ref. [26]
Voltage gain	$\frac{3D}{1-D}V_{input}$	$\frac{V_{input}}{(1-D)\frac{V_{dc}}{V_g}}$	$\frac{V_{input}}{(1-D)^3}$	$\frac{V_{input}\,(1+2d)}{1-d}$
No. of Power Switch	1	1	1	1
No. of Diodes	4	2	3	3
No. of Inductors	2	3	2	3
No. of Capacitors	6	3	2	4
Continuous Input current	Yes	Yes	Yes	Yes
Examination with a PV system (Average efficiency)	Yes, rated PV power 660W (94.7% ~ 96.5%)	Yes, rate PV power 1000 W (84.4% ~ 86.5%)	Yes, rated PV power 87 W (93% ~ 96.5%)	n/a
Examination with a fuel cell (Average efficiency)	Yes, rated fuel cell power 550 W (91.2% ~ 96.6%)	n/a	n/a	Yes, rated fuel cell power 800 W (90.5% ~ 96%)

8. Conclusion

In this paper, a new dc-dc converter is proposed to interfere with PV systems and fuel cell applications. The proposed converter has a single-switch unidirectional buck/boost operation. Compared with the conventional and recent development of relevant converters, our proposed converter does not need a complex control mechanism and can support the utilization with a continuous input current. Two different operating modes of independent and combinational power transfer sources are detailed according to the required power transfer. We have found that our converter's efficiency ranges from 93% ~ 98% while interfacing with a 600 W PV system and 91% ~ 97% while testing with a 550 W fuel cell. In both cases, the converter output voltage was stabilized at 36V to match the battery bank requirement. The maximum measured inductance current ripple is limited to under 0.70 A in both scenarios, whereas 0.16 V is the maximum output voltage ripple.

Appendix A – buck mode

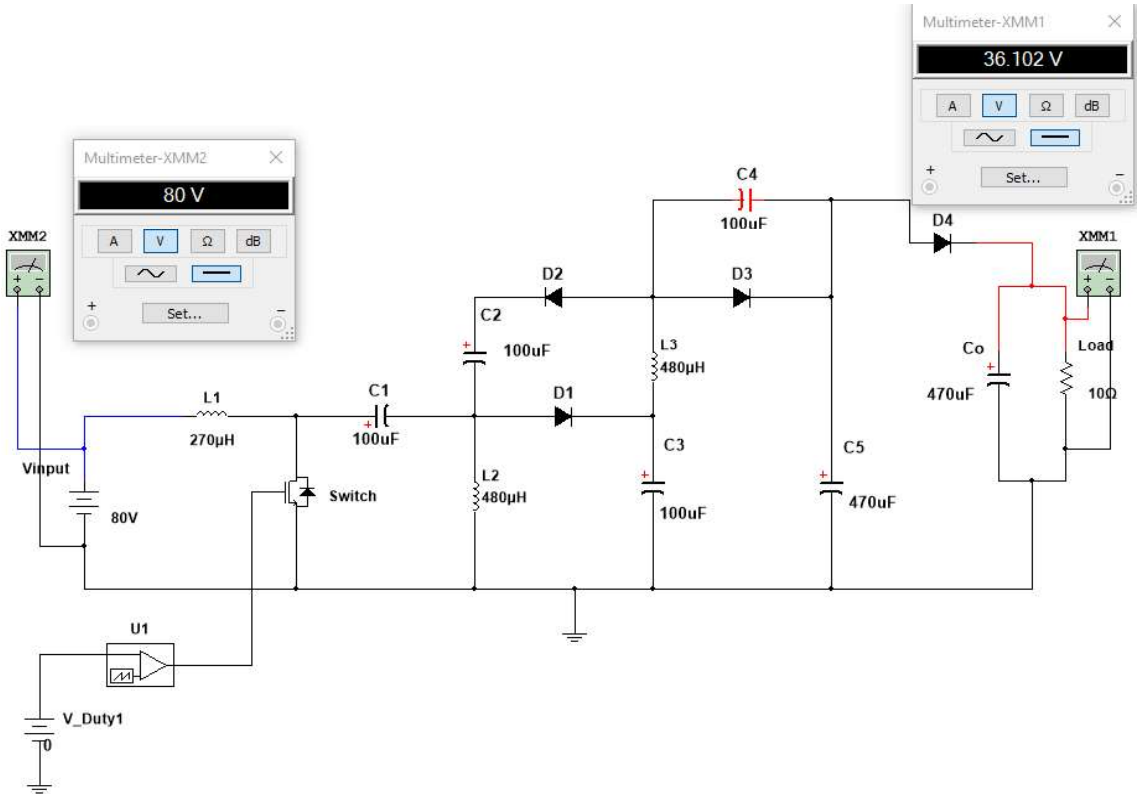

Appendix B – boost mode

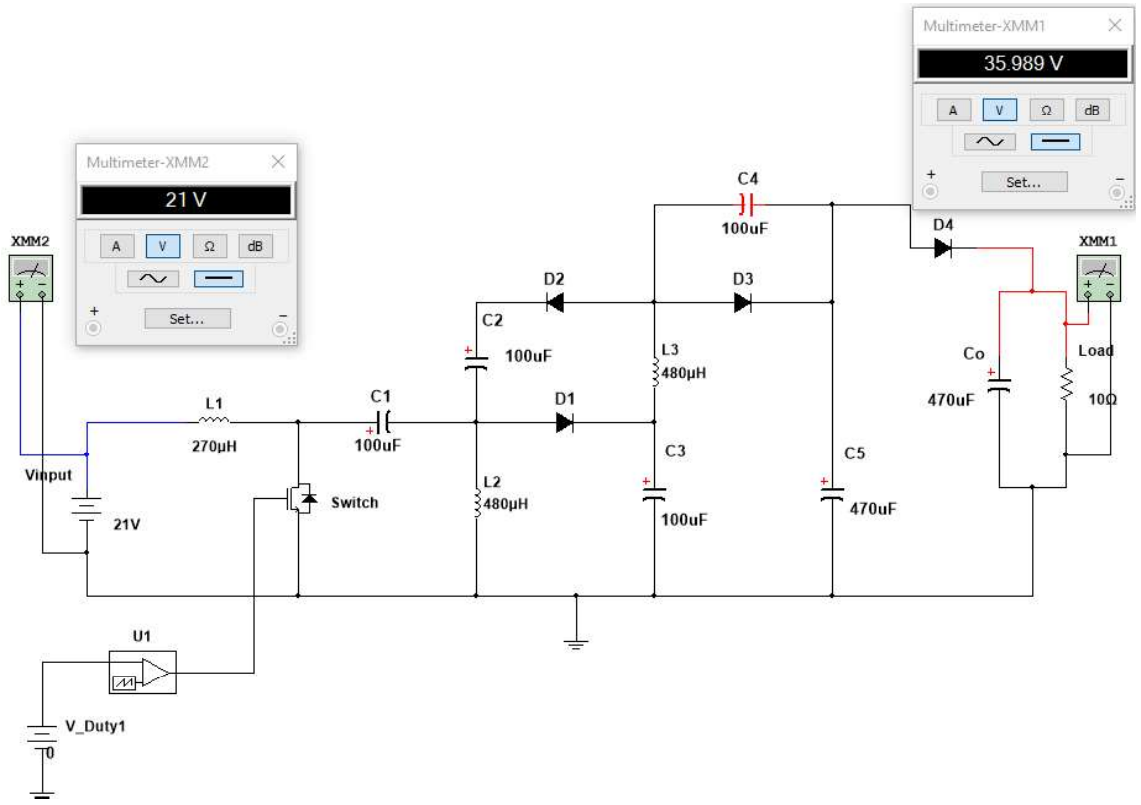

References

[1] Karthikeyan V, Gupta R. Multiple-input configuration of isolated bidirectional DC–DC converter for power flow control in combinational battery storage. IEEE Transactions on Industrial Informatics. 2017;14:2-11. https://doi.org/10.1109/TII.2017.2707106

[2] Du H, Jiang C, Wen G, Zhu W, Cheng Y. Current sharing control for parallel DC–DC buck converters based on finite-time control technique. IEEE Transactions on Industrial Informatics. 2018;15:2186-98. https://doi.org/10.1109/TII.2018.2864783

[3] Hossain MZ, Rahim NA. Recent progress and development on power DC-DC converter topology, control, design and applications: A review. Renewable and Sustainable Energy Reviews. 2018;81:205-30. https://doi.org/10.1016/j.rser.2017.07.017

[4] Kolli A, Gaillard A, De Bernardinis A, Bethoux O, Hissel D, Khatir Z. A review on DC/DC converter architectures for power fuel cell applications. Energy Conversion and Management. 2015;105:716-30. https://doi.org/10.1016/j.enconman.2015.07.060

[5] Reddy KJ, Natarajan S. Energy sources and multi-input DC-DC converters used in hybrid electric vehicle applications–A review. International journal of hydrogen energy. 2018;43:17387-408. https://doi.org/10.1016/j.ijhydene.2018.07.076

[6] Valdez-Resendiz JE, Sanchez VM, Rosas-Caro JC, Mayo-Maldonado JC, Sierra JM, Barbosa R. Continuous input-current buck-boost DC-DC converter for PEM fuel cell applications. International Journal of Hydrogen Energy. 2017;42:30389-99. https://doi.org/10.1016/j.ijhydene.2017.10.077

[7] Komurcugil H, Biricik S, Guler N. Indirect sliding mode control for DC–DC SEPIC converters. IEEE Transactions on Industrial Informatics. 2019;16:4099-108. https://doi.org/10.1109/TII.2019.2960067

[8] Siouane S, Jovanović S, Poure P. Open-switch fault-tolerant operation of a two-stage buck/buck–boost converter with redundant synchronous switch for PV systems. IEEE Transactions on Industrial Electronics. 2018;66:3938-47. https://doi.org/10.1109/TIE.2018.2847653

[9] Dhimish M. Assessing MPPT techniques on hot-spotted and partially shaded photovoltaic modules: Comprehensive review based on experimental data. IEEE Transactions on Electron Devices. 2019;66:1132-44. https://doi.org/10.1109/TED.2019.2894009

[10] Collura SM, Guilbert D, Vitale G, Luna M, Alonge F, d'Ippolito F, Scipioni A. Design and experimental validation of a high voltage ratio DC/DC converter for proton exchange membrane electrolyzer applications. International Journal of Hydrogen Energy. 2019;44:7059-72. https://doi.org/10.1016/j.ijhydene.2019.01.210

[11] Dhimish M. 70% decrease of hot-spotted photovoltaic modules output power loss using novel MPPT algorithm. IEEE Transactions on Circuits and Systems II: Express Briefs. 2019;66:2027-31. https://doi.org/10.1109/TCSII.2019.2893533

[12] Lu J, Tong X, Zeng J, Shen M, Yin J. Efficiency Optimization Design of L-LLC Resonant Bidirectional DC-DC Converter. Energies. 2021;14:3123. https://doi.org/10.3390/en14113123

[13] Gorji SA, Mostaan A, Tran My H, Ektesabi M. Non-isolated buck–boost dc–dc converter with quadratic voltage gain ratio. IET Power Electronics. 2019;12:1425-33. https://doi.org/10.1049/iet-pel.2018.5703

[14] Azer P, Emadi A. Generalized state space average model for multi-phase interleaved buck, boost and buck-boost DC-DC converters: transient, steady-state and switching dynamics. IEEE Access. 2020;8:77735-45. https://doi.org/10.1109/ACCESS.2020.2987277

[15] Litrán SP, Durán E, Semião J, Barroso RS. Single-switch bipolar output DC-DC converter for photovoltaic application. Electronics. 2020;9:1171. https://doi.org/10.3390/electronics9071171

[16] Huangfu Y, Guo L, Ma R, Gao F. An advanced robust noise suppression control of bidirectional DC–DC converter for fuel cell electric vehicle. IEEE Transactions on Transportation Electrification. 2019;5:1268-78. https://doi.org/10.1109/TTE.2019.2943895

[17] Diaz-Saldierna LH, Leyva-Ramos J, Langarica-Cordoba D, Ortiz-Lopez MG. Energy processing from fuel-cell systems using a high-gain power dc-dc converter: Analysis, design, and implementation. International Journal of Hydrogen Energy. 2021;49:25264-25276. https://doi.org/10.1016/j.ijhydene.2021.05.046

[18] Srinivasan S, Tiwari R, Krishnamoorthy M, Lalitha MP, Raj KK. Neural network based MPPT control with reconfigured quadratic boost converter for fuel cell application. International Journal of Hydrogen Energy. 2021;46:6709-19. https://doi.org/10.1016/j.ijhydene.2020.11.121

[19] Ozdemir S, Balci S, Altin N, Sefa I. Design and performance analysis of the three-level isolated DC-DC converter with the nanocyrstalline core transformer. international journal of hydrogen energy. 2017;42:17801-12. https://doi.org/10.1016/j.ijhydene.2017.02.158

[20] Concha D, Renaudineau H, Hernández MS, Llor AM, Kouro S. Evaluation of DCX converters for off-grid photovoltaic-based green hydrogen production. International Journal of Hydrogen Energy. 2021;46:19861-70. https://doi.org/10.1016/j.ijhydene.2021.03.129

[21] Bairabathina S, Balamurugan S. Review on non-isolated multi-input step-up converters for grid-independent hybrid electric vehicles. International journal of hydrogen energy. 2020;41:21687-21713. https://doi.org/10.1016/j.ijhydene.2020.05.277

[22] Huangfu Y, Ma Y, Bai H, Xu L, Wang A, Ma R. A family of high gain fuel cell front-end converters with low input current ripple for PEMFC power conditioning systems. International Journal of Hydrogen Energy. 2021;53:217156-27172. https://doi.org/10.1016/j.ijhydene.2021.05.174

[23] Slah F, Mansour A, Hajer M, Faouzi B. Analysis, modeling and implementation of an interleaved boost DC-DC converter for fuel cell used in electric vehicle. International journal of hydrogen energy. 2017;42:28852-64. https://doi.org/10.1016/j.ijhydene.2017.08.068

[24] Prabhakaran P, Agarwal V. Novel four-port dc–dc converter for interfacing solar PV–fuel cell hybrid sources with low-voltage bipolar dc microgrids. IEEE Journal of Emerging and Selected Topics in Power Electronics. 2018;8:1330-40. https://doi.org/10.1109/JESTPE.2018.2885613

[25] Ahmad J, Pervez I, Sarwar A, Tariq M, Fahad M, Chakrabortty RK, Ryan MJ. Performance Analysis and Hardware-In-the-Loop (HIL) Validation of Single Switch High Voltage Gain DC-DC Converters for MPP Tracking in Solar PV System. IEEE Access. 2020;9:48811-30. https://doi.org/10.1109/ACCESS.2020.3034310

[26] Elsayad N, Moradisizkoohi H, Mohammed OA. A Single-Switch Transformerless DC--DC Converter With Universal Input Voltage for Fuel Cell Vehicles: Analysis and Design. IEEE Transactions on Vehicular Technology. 2019;68:4537-49. https://doi.org/10.1109/TVT.2019.2905583